

Journal of Materials Chemistry A

Accepted Manuscript



This is an *Accepted Manuscript*, which has been through the Royal Society of Chemistry peer review process and has been accepted for publication.

Accepted Manuscripts are published online shortly after acceptance, before technical editing, formatting and proof reading. Using this free service, authors can make their results available to the community, in citable form, before we publish the edited article. We will replace this *Accepted Manuscript* with the edited and formatted *Advance Article* as soon as it is available.

You can find more information about *Accepted Manuscripts* in the [Information for Authors](#).

Please note that technical editing may introduce minor changes to the text and/or graphics, which may alter content. The journal's standard [Terms & Conditions](#) and the [Ethical guidelines](#) still apply. In no event shall the Royal Society of Chemistry be held responsible for any errors or omissions in this *Accepted Manuscript* or any consequences arising from the use of any information it contains.



Journal Name

ARTICLE

Porous CoP concave polyhedron electrocatalysts synthesized from metal-organic frameworks with enhanced electrochemical properties for hydrogen evolution

Received 00th January 20xx,
Accepted 00th January 20xx

DOI: 10.1039/x0xx00000x

www.rsc.org/

Miao Xu,^{a,b} Lei Han,^{a,b} Yujie Han,^{a,b} You Yu,^{a,b} Junfeng Zhai,^a and Shaojun Dong^{a,b,*}

Developing highly-efficient and low-cost noble metal-free catalysts toward hydrogen evolution from water splitting is an attractively alternative strategy to solve the ever-increasing environmental contamination and energy demand. Herein, the porous CoP electrocatalyst with a concave polyhedron (CPH) structure was facilely prepared by a topological conversion strategy using Co-MOFs (ZIF-67) polyhedrons as the precursor. The morphology of Co-MOFs is well inherited by the as-prepared CoP sample due to the multi-step calcination process at low temperature, which imaginably results in the formation of a porous structure. Compared with the contrastive CoP nanoparticles (NPs), the obtained porous CoP CPHs electrocatalyst exhibit a remarkably enhanced electrocatalytic performance with a current density of 10 mA cm⁻² at an overpotential of 133 mV and a superior durability for hydrogen evolution reaction (HER) in acid media. A small Tafel slope of ca. 51 mV dec⁻¹ reveals a Volmer-Heyrovsky mechanism during the HER. This work provided a new insight to fabricate morphology-controlled transition metal phosphides with a porous structure *via* topological conversion, which have important potential applications, such as electrocatalysis, photocatalysis and sensor, thanks to its porosity and controllability.

Introduction

Environmentally-friendly energy production has been urgent and received much attention in the past decades due to the ever-increasing environmental contamination and energy demand. Hydrogen has been recognized as an ideal alternative energy to replace fossil fuels in the future because of its green and renewable features as well as high energy capacity^{1, 2}. Electrocatalytic water splitting for hydrogen production is a direct and attractive strategy, which requires highly efficient electrocatalysts to get high current density at low overpotential in the hydrogen evolution reaction (HER) with no harmful by-products release^{3, 4}. Traditional platinum (Pt) based materials have been regarded as the most active and stable catalysts for the HER, nevertheless, its high cost limits its widespread applications in energy conversion⁵⁻⁹. Therefore, developing noble metal-free catalysts with a great activity and a long-term stability for HER is an urgent and challenging task.

Transition-metal phosphides (TMPs) have been recently applied for electrocatalytic hydrogen evolution driving from

the fact that they can bind with protons to promote hydrogen formation¹⁰⁻¹⁵. Cobalt phosphide (CoP) has been demonstrated as an efficient electrocatalyst for hydrogen evolution, of which the electrocatalytic performances greatly rely on the microstructures of the catalysts. Therefore, numerous researchers concentrate on the fabrication of CoP with different morphologies such as one dimensional (1D) CoP nanowires or nanorods^{16, 17}, hierarchical nanostructures¹⁸ and nanoparticles^{13, 19}, *etc.*, by either low temperature phosphidation²⁰ or electrochemical method²¹ using cobalt oxides^{16, 20} and cobalt nanoparticles¹³ as the precursors, respectively. Compared with the above morphologies, porous materials usually possess unique and fascinating catalytic performances in many fields because of their large surface area, thin pore wall and many active sites, and so on²²⁻²⁵. So far, porous CoP polyhedrons have not yet been obtained due to the inevitable coalescence of nanoparticles at the calcination process.

Metal-organic frameworks (MOFs) are a new class of organic-inorganic hybrid materials, which have high porosity and special morphologies, of which the particle size can be easily tuned by changing transition-metal ions and organic ligands²⁶⁻²⁸. Thus, MOFs have generally been demonstrated as a promising precursor to fabricate carbon nanostructures or porous metal oxides by a simple through solid-state thermolysis process^{29, 30}. Tang *et al.* reported carbonized nanoparticles, which has been produced *via* pyrolysis of monodisperse MOFs (MIL-88B-NH₃) as a highly efficiently oxygen reduction reaction (ORR)³⁰. Lou *et al.* have synthesized

^a State Key Laboratory of Electroanalytical Chemistry, Changchun Institute of Applied Chemistry, Chinese Academy of Science, Changchun, Jilin, 130022 (PR China). E-mail: dongsj@ciac.ac.cn

^b University of Chinese Academy of Sciences, Beijing, 100049 (PR China).

† Electronic Supplementary Information (ESI) available: [additional characterization, including XPS survey spectrum, HRTEM image, SEM images, polarization curves and EIS spectrum.]. See DOI: 10.1039/x0xx00000x

porous molybdenum carbide nano-octahedrons by confined carburization on MOFs at 800 °C, which exhibits a highly electrocatalytic activity in HER³¹. Nevertheless, to the best of our knowledge, less attention has so far been paid on the fabrication of TMPs based on MOFs with the similar structural features, even though Ni₂P nanoparticles have been obtained from a Ni-based MOF³². Since the structure of the Ni-based MOF has been totally broken up in the directly phosphatizing and the obtained Ni₂P is composed of irregular nanoparticles, the enhancement of the electrocatalytic activity is limited.

Herein, we have for the first time synthesized porous CoP concave polyhedrons (CoP CPHs) by a facilely topological conversion strategy of a low temperature multi-step calcination using Co-MOFs polyhedrons (ZIF-67) as the precursor. In this strategy, the as-prepared CoP CPHs well inherit the morphology of Co-MOFs and exhibit the porosity and regular concave polyhedron morphology. As a consequence, the obtained porous CoP CPHs offer an attractively enhanced electrocatalytic performance and durability for hydrogen evolution in acid media compared with the contrastive CoP nanoparticles (NPs). An overpotential of 133 mV at a current density of 10 mA cm⁻² and a small Tafel slope of ca. 51 mV dec⁻¹ have been obtained, suggesting a possible Volmer-Heyrovsky mechanism during the HER. Thus, in this work, we have for the first time fabricated CoP CPHs for HER and this multi-step topological conversion strategy can be extended into the controlled synthesis of porous nanostructures of TMPs.

Experimental

Chemicals

Cobalt nitrate hexahydrate (Co(NO₃)₂·6H₂O) was obtained from Beijing Chemical Works, P. R. China. 2-Methylimidazole (C₄H₆N₂) and sodium hypophosphite (NaH₂PO₂) were purchased from Aladdin. Commercial Pt/C (20 wt%) catalyst and Nafion ethanol solution (5 wt%) were purchased from Alfa Aesar. All chemicals were used as received without further purification and all aqueous solutions were prepared with ultrapure water (>18.25 MΩ cm) obtained from Millipore system.

Characterization

The X-ray diffraction (XRD) measurements were performed on a D8 Focus diffractometer (Bruker) with Cu Kα radiation (λ = 0.15405 nm) in the range of 10–80° (2θ). X-ray photoelectron spectroscopy (XPS) analysis was carried on an ESCALAB MK II X-ray photoelectron spectrometer. A XL30 ESEM scanning electron microscope (SEM) was used to determine the morphology and composition of products. Transmission electron microscopy (TEM) measurements were made on a HITACHI H-8100 EM with an accelerating voltage of 200 kV. High-resolution transmission electron microscopy (HRTEM) measurements, high-angle annular dark-field scanning TEM (HAADF-STEM), and elemental mapping were made on a JEM-2100F high-resolution transmission electron microscope

operating at 200 kV. The electrochemical impedance spectroscopy (EIS) measurements were carried out by a Zennium electrochemical workstation (Zahner, Germany). N₂ adsorption-desorption analysis was performed on an AutosorbStation1 (Quantachrome, USA).

Synthesis of Co-MOFs

The Co-MOFs (ZIF-67) precursors were first synthesized *via* a simple method according to the previous report³³. In a typical synthesis, 3 mL Co(NO₃)₂·6H₂O (0.52 M) solution was added into 20 mL aqueous solution of 2-methylimidazole (3.36 M) under stirring, and the mixture was held at room temperature (25 °C) for 6 h with continuous stirring. The obtained purple precipitate was collected by centrifugation and washed with ethanol for three times. Finally, the solid product was dried at 80 °C overnight.

Synthesis of porous Co₃O₄ and CoP CPHs

The typical preparation procedure of the porous CoP electrocatalysts had two steps, involving the fabrication of porous Co₃O₄ from the Co-MOFs (ZIF-67) and the subsequent phosphorization procedure *via* calcination treatment. In the first step, the as-prepared Co-MOFs (ZIF-67) precursors were heated at 300 °C for 3 h in air with a heating rate of 5 °C/min and the resulting black products was porous Co₃O₄. After that, 10 mg porous Co₃O₄ and 200 mg NaH₂PO₂ were placed at two separate positions in one quartz boat with NaH₂PO₂ at the upstream side of the furnace. Then, the samples were heated to 300 °C for 2 h with a heating rate of 2 °C /min in N₂ atmosphere. After cooling to room temperature, the porous CoP was collected.

Synthesis of Co₃O₄ and CoP nanoparticles

Co₃O₄ NPs were prepared by calcining 100 mg Co(NO₃)₂·6H₂O at 300 °C for 3h with a heating rate of 5 °C/min in air. Furthermore, to convert Co₃O₄ NPs to CoP NPs, the same phosphidation procedure was used.

Preparation of working electrodes

5 mg of the catalyst was dispersed in 1 mL water/ethanol mixed solvent (v/v = 1:1) solution which containing 10 μL of Nafion (5 wt%) on solution and sonicated for at least 30 min to get a homogeneous catalyst ink. Prior to the surface coating, the glassy carbon electrode (GCE, 3 mm in diameter) was polished carefully with 1.0, 0.3 and 0.05 μm alumina powder, respectively, and rinsed with ultrapure water, followed by sonicated in ethanol and ultrapure water successively. Then, the electrode was allowed to dry under N₂. After that, 5 μL of the catalyst ink was dropped on the surface of GCE (loading ~ 0.35 mg/cm²) and dried at room temperature before electrochemical measurements.

Electrochemical measurements

Electrochemical experiments (Linear sweep voltammetry and Amperometric i-t curve) were performed on a CHI 832c

electrochemical analyzer (CH Instruments, Chenhua Co., Shanghai, China) at room temperature (25 °C). A conventional three-electrode cell was used, including an Ag/AgCl (saturated KCl) electrode as reference electrode, a platinum foil as counter electrode, and the bare and modified GCE as working electrode. All the measurements were performed in an electrolyte solution of 0.5 M H₂SO₄ solution. Line sweep voltammetry (LSV) curves were measured at a sweep rate of 2 mV s⁻¹ to obtain the polarization curves. Unless otherwise specified, the current density was normalized to the geometrical area and the potentials are reported versus reversible hydrogen electrode (RHE) by converting the measured potentials vs Ag/AgCl according to the Nernst equation: $ERHE = E_{Ag/AgCl} + 0.059 \text{ pH} + 0.197$. The stability tests were performed by cyclic voltammetry from +0.02 V to -0.286 V vs. RHE with the sweep rate of 100 mV s⁻¹.

Results and discussion

Preparation and characterization of the CoP CPHs

Fig. 1 is the morphology and structure characterizations of the as-prepared CoP CPHs. From the SEM image in **Fig. 1A**, it can be easily observed that as-prepared sample shows well-dispersed and polyhedron (PH) nanostructures with an overall size of 100 – 250 nm. Close observation in **Fig. 1B** shows that the surface of the as-prepared PHs is concave and fairly rough, indicating its porosity. **Fig. 1C** displays the TEM image of the as-prepared sample. The differentia of the contrast grade distinctly reveals its highly porous texture throughout the whole particles, which is caused by numerous primary crystallites randomly attached with each other. The HRTEM

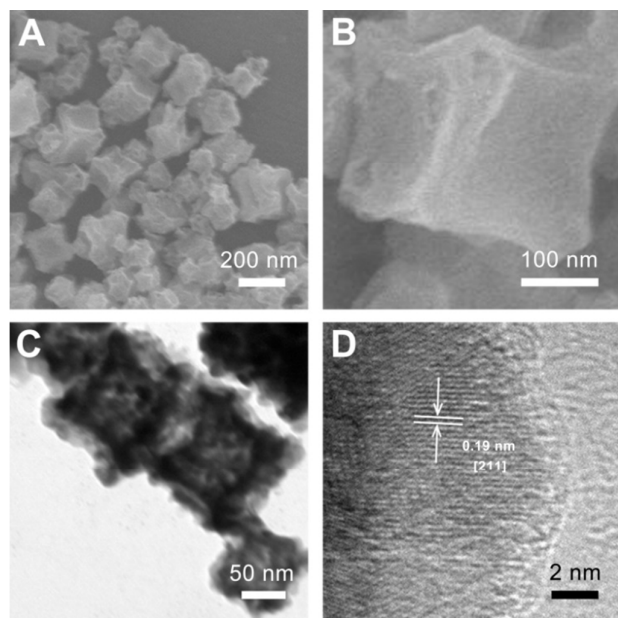


Fig. 1 Low- (A) and high-magnification SEM images (B), TEM image (C) and HRTEM image (D) of the as-obtained CoP CPHs.

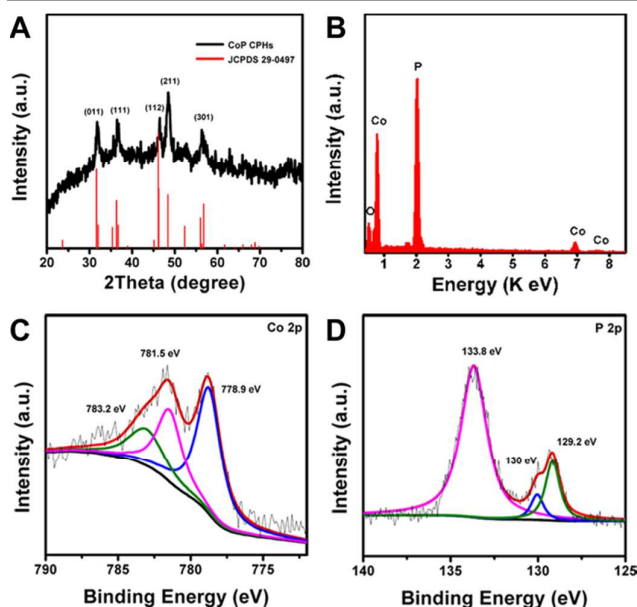


Fig. 2 XRD patterns (A), EDX pattern (B), high resolution Co (C) and P (D) XPS spectra of the as-obtained CoP CPHs.

images (**Fig. 1D**) indicate the interplanar spacing of 0.19 nm, which is assigned to the plane (211) of CoP (JCPDS card No. 29-0497). Additionally, more HRTEM images including the lattice fringes are shown in **Fig. S2**.

More composition information of the as-prepare CPHs has been obtained by XRD, EDX, HAADF-STEM and XPS characterization. The XRD diffraction peaks (**Fig. 2A**) can be respectively assigned to the (011), (111), (112), (211) and (301) facets of CoP according to JCPDS card No. 29-0497 without other diffraction peaks detected. The broader diffraction peaks with a lower intensity suggests its ultrafine crystalline size. The elements Co, P and O are obviously detected in the sample by EDX (**Fig. 2B**) and the element O may come from the absorbed O species in air. The STEM results show that the Co and P elements are well-distributed in a single CPH (**Fig. S3**). The XPS spectrum of element Co can be deconvoluted into three Gaussian-Lorentzian peaks located at 778.9, 781.5, and 783.2 eV, respectively (**Fig. 2C**). The peak at 778.9 eV is identical to CoP and the peaks at 781.5 and 783.2 eV are the satellite peaks arising from plasmon loss processes³⁴. **Fig. 2D** shows the P XPS spectrum, which can also be split into peaks at binding energies of 129.2 and 130.0 eV corresponding to P 2p_{3/2} and P 2p_{1/2}³⁴, and the other P 2p peak centered at 133.8 eV, which is assigned to the oxidized phosphorus species, such as PO₄³⁻ or P₂O₅, arising from the inescapable contact between CoP surface and air^{35, 36}. This result further confirms the generation of CoP. Compared with the binding energies of metal Co 2p_{3/2} (778.1 eV) and the elemental P (130.2 eV)²⁰, the positive and negative shifts of Co 2p_{3/2} (778.9 eV) and P 2p_{3/2} (129.2 eV) in the as-prepared porous CoP CPHs imply a charge transfer from Co to P^{34, 37}. This, in combination with the morphology and structure characterization, manifests that the porous CoP CPHs have been simply synthesized by a facilely topological conversion strategy based on Co-MOFs as the precursor.

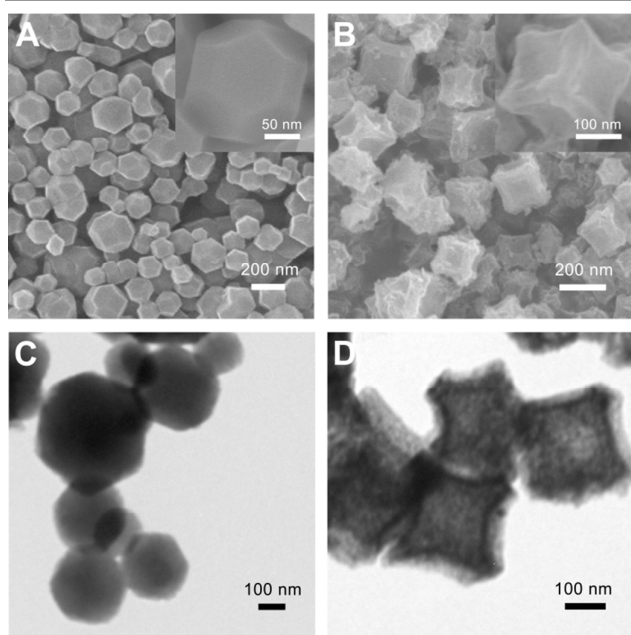


Fig. 3 SEM images (A and B) and TEM images (C and D) of Co-MOFs (ZIF-67) (A and C) and Co_3O_4 CPHs (B and D).

Formation process of as-prepared CoP CPHs

To clear the formation process of the as-prepared porous CoP CPHs, the morphologies and structures of the original Co-MOFs precursors and the corresponding intermediate oxides have been characterized by SEM, TEM, and XRD techniques. **Fig. 3A** and **C** show the SEM and TEM images of the original Co-MOFs precursors. Regular polyhedral particles with a particle size of 100 – 300 nm are observed. The high-magnification SEM image shows the surfaces of the PHs are slightly concave (**Fig. 3C**). The XRD pattern in **Fig. 4** (curve a) demonstrates that the Co-MOFs precursors are ZIF-67, which are zeolitic imidazolate framework materials^{33, 38, 39}. After the

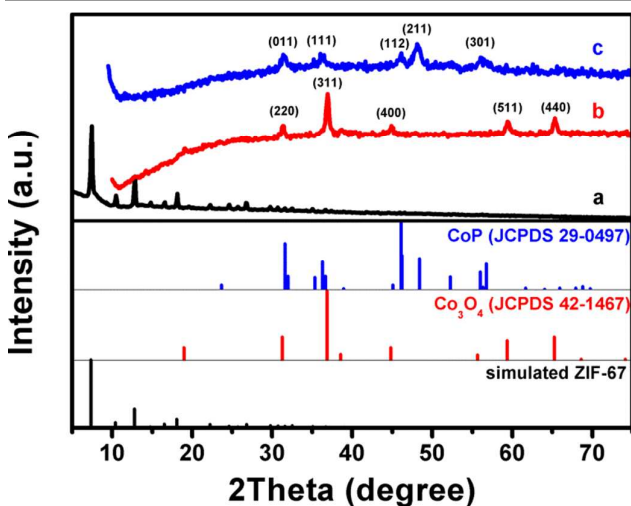


Fig. 4 XRD patterns of Co-MOFs (ZIF-67) (a), Co_3O_4 CPHs (b) and CoP CPHs (c).

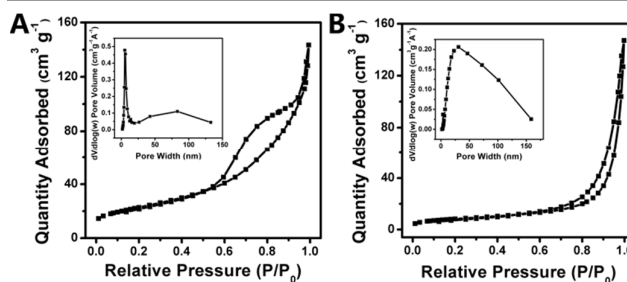


Fig. 5 N_2 adsorption-desorption isotherms and the corresponding pore size-distribution profiles (inset) of Co_3O_4 CPHs (A) and CoP CPHs (B).

subsequent carbonization step in air at 300 °C, the surface of obtained particles collapses and displays like CPHs as shown in **Fig. 3B**. Compared with the original Co-MOFs, the obtained products exhibit a distinctly concave surface. The diffraction peaks of the products can be unambiguously indexed to the (220), (311), (400), (511) and (440) planes of Co_3O_4 (JCPDS 42-1467), respectively (**Fig. 4**, curve b). In addition, TEM image (**Fig. 3D**) of Co_3O_4 CPHs suggests the particles are composed of lots of small crystallites and possess a clear pore structure as same as the porous CoP CPHs. The HRTEM measurement is carried out and the measured the lattice plane is about 0.24 nm (**Fig. S4**), indexing to the (311) plane of Co_3O_4 . Following with the transformation from Co-MOFs to Co_3O_4 , organic ligands and some absorbed molecules in the Co-MOF polyhedral precursors are decomposed to release CO_2 , H_2O , and NO_x . On the other hand, the residual Co^{2+} ions react with O_2 to form Co_3O_4 frameworks³³. This unquestionably results the structural strain to form further concave surface and porous structure. Followed the subsequent low-temperature phosphorization process in a non-oxygen environment, P atoms are introduced into the crystal lattice of Co_3O_4 to substitute O atoms to generated CoP without the change of the particle structures.

To elucidate the transformation of porous structures during the topological conversion, the nitrogen adsorption-desorption isotherms of the as-prepared CoP and Co_3O_4 CPHs are performed and the results are displayed in **Fig. 5**. Both samples exhibit a typical type-IV isotherm, indicating the mesoporosities of the two samples. The Barrette-Joyner-Halenda (BJH) pore-size distribution in **Fig. 5A** (inset) shows that the pore distribution of the as-prepared Co_3O_4 CPHs are mainly concentrate at approximately 5 nm. As for the as-prepared CoP CPHs, the pores become bigger during the low-temperature phosphorization with a predominant size of ca. 30 nm (**Fig. 5B**, inset). Correspondingly, the Brunauer-Emmett-Teller (BET) special surface area of CoP CPHs is calculated to be 29.42 $\text{m}^2 \text{g}^{-1}$, which is lower than that of Co_3O_4 CPHs (81.65 $\text{m}^2 \text{g}^{-1}$). The increased pore size and decreased special surface area of the as-prepared CoP CPHs compared with the Co_3O_4 CPHs can be explained by its increased crystallite of the as-prepared CoP CPHs during the second phosphorization calcination process followed by several pores blocked up or collapse.

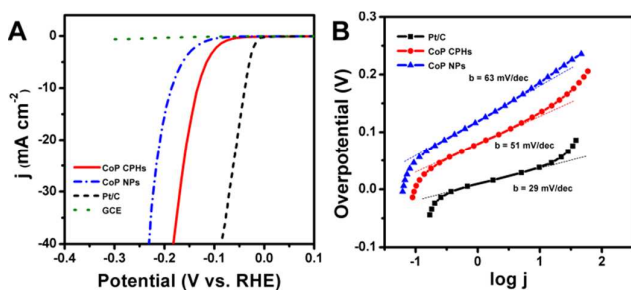


Fig. 6 (A) Polarization curves of bare GCE, Pt/C, CoP NPs and CoP CPHs in 0.5 M H₂SO₄ at the scan rate of 2 mV s⁻¹. (B) Tafel plots of Pt/C, CoP NPs and CoP CPHs.

Electrocatalytic Activity

The electrocatalytic HER activities of the as-prepared porous CoP CPHs are evaluated in 0.5 M H₂SO₄ at scan rate of 2 mV s⁻¹ in a typical three-electrode system. For comparison, the prepared contrastive CoP nanoparticles (NPs) are shown in **Fig. S5**. **Fig. 6A** shows the polarization curves, which are obtained by linear sweep voltammetry (LSV) measurement. The activities of bare glassy carbon electrode (GCE), commercial Pt/C, and CoP NPs are also investigated under the same conditions. As expected, the blank experiment of bare GCE has not displayed obvious cathodic catalytic current for HER in the range from 0 V to -0.3 V (vs. RHE), while the commercial Pt/C modified electrode has the best electrocatalytic activity toward HER with the overpotential approximately equal to zero (**Fig. S6**). With regard to the prepared porous CoP CPHs electrocatalysts, it has low onset overpotential of *ca.* 30 mV (**Fig. S6**). And if the overpotential further increases, the value of cathodic current will quick raise. The porous CoP CPHs electrocatalyst only needs an overpotential of 133 mV to reach the current density of 10 mA cm⁻², whereas the contrasted CoP NPs exhibit an overpotential of 187 mV under the same condition. That is to say, the porous CoP CPHs electrocatalysts have better electrocatalytic performance than the contrastive CoP NPs prepared *via* a direct calcination. By means of using MOFs as the precursors, the synthesized CoP CPHs electrocatalysts possess porous structure, which is beneficial to exposing more active centers for enhance the electrocatalytic activity. At the same time, the existent pores can make the electrolyte diffusion faster, as evidenced by the much smaller semicircle of the as-prepared CoP CPHs than that of CoP NPs in the Nyquist plots of electrochemical impedance spectra (EIS) shown in **Fig. S7**, reflecting its charge transfer resistance. Consequently, the porous CoP CPHs electrocatalysts have enhanced electrochemical properties toward HER. Additionally, the electrocatalytic performance of the porous CoP CPHs are superior to most of reported non-noble metal based catalysts toward HER, for example, CoP microspheres²⁰, porous FeP nanosheets¹¹, WS₂ nanoribbons⁴⁰, defect-rich MoS₂ ultrathin nanosheets⁴¹, and so on^{14, 42-47} (**Table S1**).

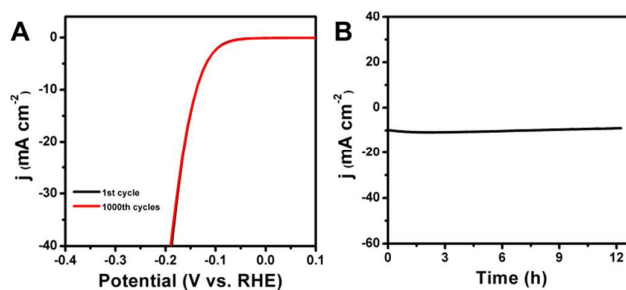


Fig. 7 (A) Polarization curves of CoP CPHs before and after 1000 cycles at the scan rate of 100 mV s⁻¹ between 0.02 V and -0.286 V. (B) The current-time curve of the CoP CPHs measured at an overpotential of 130 mV in 0.5 M H₂SO₄.

Fig. 6B exhibits the Tafel plots of the as-prepared porous CoP CPHs, commercial Pt/C and the contrastive CoP NPs. The linear region may fit for the Tafel equation: $\eta = b \log j + a$, where j is current density, a is the Tafel constant and b is the Tafel slope. On the basis of the Tafel equation, we can figure out the Tafel slopes of Pt/C, CoP NPs, and porous CoP CPHs are 29, 63, and 51 mV dec⁻¹, respectively. Generally, in acidic media, cathodic HER has the following steps: the Volmer step: $\text{H}_3\text{O}^+ + \text{e}^- \rightarrow \text{H}_{\text{ads}} + \text{H}_2\text{O}$, followed by the Heyrovsky step: $\text{H}_{\text{ads}} + \text{H}_3\text{O}^+ + \text{e}^- \rightarrow \text{H}_2 \uparrow + \text{H}_2\text{O}$ or the Tafel step: $2 \text{H}_{\text{ads}} \rightarrow \text{H}_2 \uparrow$ (where H_{ads} is an adsorbed H intermediate)⁴⁸. And the Tafel slopes are 116, 38, and 29 mV dec⁻¹ for Volmer, Heyrovsky, and Tafel step, respectively⁴⁹. Therefore, the Tafel slope of the porous CoP CPHs indicating that corresponding HER abides by a Volmer-Heyrovsky mechanism. We can also deduce the exchange current density (j_0) from the Tafel plot when the overpotential value is 0 V (vs. RHE). On these grounds, the j_0 of porous CoP CPHs is calculated as 4.4×10^{-2} mA cm⁻² (**Fig. S8**), which is larger than many reported literatures^{40-42, 45-47}.

Stability Evaluation

Furthermore, the as-prepared porous CoP CPHs also perform in 0.5 M H₂SO₄ to examine the stability. **Fig. 7A** shows the polarization curves of the porous CoP CPHs electrode before and after 1000 continuous cyclic voltammetry (CV) cycles between 0.02 V and -0.286 V (vs. RHE) with the scan rate of 100 mV s⁻¹. Compared between the first and final cycles of porous CoP CPHs electrocatalysts, there is negligible loss of the current density in the polarization curves, indicating the porous CoP CPHs are a kind of stable HER electrocatalysts in acid media. Meanwhile, we test the long-term stability of the CoP CPHs electrocatalysts for *ca.* 12h at a static overpotential of 130 mV (vs. RHE) (**Fig. 7B**). After 12h, the current density has no obvious decrease, suggesting its superior durability. Furthermore, the overpotential is increased to 200 mV implying a larger current density of ~ 50 mA cm⁻², which further verify the excellent stability of the as-prepared CoP CPHs (**Fig. S9**). **Fig. S10** shows the morphology, structure and composition characterizations of the recycling CoP CPHs. The results reveal that the recycling sample maintains the concave polyhedron structure and the similar composition after the electrocatalysis.

The EDX results in **Table S2** indicate the atom ratios of Co and P before and after electrocatalysis are both *ca.* 1 : 1. Overall, the as-prepared CoP CPHs have good structural stability and electrocatalytic durability.

Conclusions

In summary, we synthesize the porous CoP CPHs by a facilely topological conversion method *via* a low-temperature multi-step calcination reactions. The obtained porous nanostructural CoP electrocatalysts are of concave polyhedron morphology and have improved electrocatalytic activity toward HER. In acid media, the CoP CPHs electrocatalysts have a low onset potential of *ca.* 30 mV, an exchange current density of 4.4×10^{-2} mA cm⁻², and a Tafel slope of *ca.* 51 mV dec⁻¹. Meanwhile, it merely needs overpotential of 133 mV to drive current of 10 mA cm⁻². Furthermore, the prepared material has a good long-term stability and its electrocatalytic activity can last at least 12 hours in H₂SO₄. This work promotes a new insight for preparing porous and morphology-controlled TMPs, which are promising for highly efficient electrocatalytic and photocatalytic hydrogen production, *via* topological conversion strategy based on MOFs.

Acknowledgements

This work was supported by the National Natural Science Foundation of China (No. 21375123), the 973 Project (No. 2011CB911002) and the Ministry of Science and Technology of China (No. 2013YQ170585).

Notes and references

- N. S. Lewis and D. G. Nocera, *Proc. Natl. Acad. Sci. USA*, 2006, **103**, 15729-15735.
- M. G. Walter, E. L. Warren, J. R. McKone, S. W. Boettcher, Q. Mi, E. A. Santori and N. S. Lewis, *Chem. Rev.*, 2010, **110**, 6446-6473.
- X. Zou and Y. Zhang, *Chem. Soc. Rev.*, 2015, DOI: 10.1039/c4cs00448e.
- X. Huang, Y. Zhao, Z. Ao and G. Wang, *Sci. Rep.*, 2014, **4**, 7557.
- N. M. Marković, B. N. Grgur and P. N. Ross, *J. Phys. Chem. B*, 1997, **101**, 5405-5413.
- R. Subbaraman, D. Tripkovic, D. Strmcnik, K. C. Chang, M. Uchimura, A. P. Paulikas, V. Stamenkovic and N. M. Markovic, *Science*, 2011, **334**, 1256-1260.
- W. Sheng, H. A. Gasteiger and Y. Shao-Horn, *J. Electrochem. Soc.*, 2010, **157**, B1529-B1536.
- D. V. Esposito, S. T. Hunt, Y. C. Kimmel and J. G. Chen, *J. Am. Chem. Soc.*, 2012, **134**, 3025-3033.
- X. Cao, Y. Han, C. Gao, Y. Xu, X. Huang, M. Willander and N. Wang, *Nano Energy*, 2014, **9**, 301-308.
- J. M. McEnaney, J. C. Crompton, J. F. Callejas, E. J. Popczun, A. J. Biacchi, N. S. Lewis and R. E. Schaak, *Chem. Mater.*, 2014, **26**, 4826-4831.
- Y. Xu, R. Wu, J. Zhang, Y. Shi and B. Zhang, *Chem. Commun.*, 2013, **49**, 6656-6658.
- C. A. C. Sequeira, D. M. F. Santos and P. S. D. Brito, *Energy Environ. Sci.*, 2011, **36**, 847-853.
- E. J. Popczun, C. G. Read, C. W. Roske, N. S. Lewis and R. E. Schaak, *Angew. Chem. Int. Ed.*, 2014, **53**, 5427-5430.
- J. Tian, Q. Liu, N. Cheng, A. M. Asiri and X. Sun, *Angew. Chem. Int. Ed.*, 2014, **53**, 9577-9581.
- Z. Pu, Q. Liu, A. M. Asiri and X. Sun, *ACS Appl. Mater. Interfaces*, 2014, **6**, 21874-21879.
- J. Tian, Q. Liu, A. M. Asiri and X. Sun, *J. Am. Chem. Soc.*, 2014, **136**, 7587-7590.
- Z. Huang, Z. Chen, C. Lv, M. G. Humphrey and C. Zhang, *Nano Energy*, 2014, **9**, 373-382.
- E. J. Popczun, C. W. Roske, C. G. Read, J. C. Crompton, J. M. McEnaney, J. F. Callejas, N. S. Lewis and R. E. Schaak, *J. Mater. Chem. A*, 2015, **3**, 5420-5425.
- J. F. Callejas, C. G. Read, E. J. Popczun, J. M. McEnaney and R. E. Schaak, *Chem. Mater.*, 2015, **27**, 3769-3774.
- Q. Liu, J. Tian, W. Cui, P. Jiang, N. Cheng, A. M. Asiri and X. Sun, *Angew. Chem. Int. Ed.*, 2014, **53**, 6710-6714.
- F. H. Saadi, A. I. Carim, E. Verlage, J. C. Hemminger, N. S. Lewis and M. P. Soriaga, *J. Phys. Chem. C*, 2014, **118**, 29294-29300.
- C. M. Parlett, K. Wilson and A. F. Lee, *Chem. Soc. Rev.*, 2013, **42**, 3876-3893.
- R. J. White, V. Budarin, R. Luque, J. H. Clark and D. J. Macquarrie, *Chem. Soc. Rev.*, 2009, **38**, 3401-3418.
- J. Zhang and C. M. Li, *Chem. Soc. Rev.*, 2012, **41**, 7016-7031.
- Z. Tian, *Science*, 1997, **276**, 926-930.
- C. Sanchez, P. Belleville, M. Popall and L. Nicole, *Chem. Soc. Rev.*, 2011, **40**, 696-753.
- S. L. James, *Chem. Soc. Rev.*, 2003, **32**, 276-288.
- F. A. Paz, J. Klinowski, S. M. Vilela, J. P. Tome, J. A. Cavaleiro and J. Rocha, *Chem. Soc. Rev.*, 2012, **41**, 1088-1110.
- X. Xu, R. Cao, S. Jeong and J. Cho, *Nano Lett.*, 2012, **12**, 4988-4991.
- S. Zhao, H. Yin, L. Du, L. He, K. Zhao, L. Chang, G. Yin, H. Zhao, S. Liu and Z. Tang, *ACS Nano*, 2014, **8**, 12660-12668.
- H. B. Wu, B. Y. Xia, L. Yu, X. Y. Yu and X. W. Lou, *Nat. Commun.*, 2015, **6**, 6512.
- T. Tian, L. Ai and J. Jiang, *RSC Adv.*, 2015, **5**, 10290-10295.
- Y. Lu, W. Zhan, Y. He, Y. Wang, X. Kong, Q. Kuang, Z. Xie and L. Zheng, *ACS Appl. Mater. Interfaces*, 2014, **6**, 4186-4195.
- A. P. Grosvenor, S. D. Wik, R. G. Cavell and A. Mar, *Inorg. Chem.*, 2005, **44**, 8988-8998.
- J. Bai, X. Li, A. Wang, R. Prins and Y. Wang, *J. Catal.*, 2012, **287**, 161-169.
- J. Wang, Q. Yang, Z. Zhang and S. Sun, *Chem.-Eur. J.*, 2010, **16**, 7916-7924.
- A. W. Burns, K. A. Layman, D. H. Bale and M. E. Bussell, *Appl. Catal., A*, 2008, **343**, 68-76.
- N. L. Torad, M. Hu, S. Ishihara, H. Sukegawa, A. A. Belik, M. Imura, K. Ariga, Y. Sakka and Y. Yamauchi, *Small*, 2014, **10**, 2096-2107.
- Q. Shi, Z. Chen, Z. Song, J. Li and J. Dong, *Angew. Chem. Int. Ed.*, 2011, **50**, 672-675.
- J. Lin, Z. Peng, G. Wang, D. Zakhidov, E. Larios, M. J. Yacaman and J. M. Tour, *Adv. Energy Mater.*, 2014, **4**, 1301875.
- J. Xie, H. Zhang, S. Li, R. Wang, X. Sun, M. Zhou, J. Zhou, X. W. Lou and Y. Xie, *Adv. Mater.*, 2013, **25**, 5807-5813.
- P. Xiao, M. A. Sk, L. Thia, X. Ge, R. J. Lim, J.-Y. Wang, K. H. Lim and X. Wang, *Energy Environ. Sci.*, 2014, **7**, 2624-2629.
- Y. Bai, H. Zhang, X. Li, L. Liu, H. Xu, H. Qiu and Y. Wang, *Nanoscale*, 2015, **7**, 1446-1453.
- J. M. McEnaney, J. C. Crompton, J. F. Callejas, E. J. Popczun, C. G. Read, N. S. Lewis and R. E. Schaak, *Chem. Commun.*, 2014, **50**, 11026-11028.
- A. Lu, Y. Chen, H. Li, A. Dowd, M. B. Cortie, Q. Xie, H. Guo, Q. Qi and D.-L. Peng, *Int. J. Hydrogen Energy*, 2014, **39**, 18919-18928.

Journal Name

ARTICLE

- 46 H. Vrubel and X. Hu, *Angew. Chem. Int. Ed.*, 2012, **51**, 12703-12706.
- 47 W. F. Chen, K. Sasaki, C. Ma, A. I. Frenkel, N. Marinkovic, J. T. Muckerman, Y. Zhu and R. R. Adzic, *Angew. Chem. Int. Ed.*, 2012, **51**, 6131-6135.
- 48 B. E. Conway and B. V. Tilak, *Electrochim. Acta*, 2002, **47**, 3571-3594.
- 49 N. Pentland, J. O. Bockris and E. Sheldon, *J. Electrochem. Soc.*, 1957, **104**, 182-194.

Graphical Abstract

